Cellular Signalling 54 (2019) 179–190

Contents lists available at ScienceDirect

Cellular Signalling

journal homepage: www.elsevier.com/locate/cellsig

Neuroprotective effects of overexpressed microRNA-200a on activation of glaucoma-related retinal glial cells and apoptosis of ganglion cells *via* downregulating FGF7-mediated MAPK signaling pathway

Hui Peng, Ya-Bin Sun, Ji-Long Hao, Cheng-Wei Lu, Ming-Chao Bi, E. Song*

Department of Ophthalmology, First Hospital of Jilin University, No. 71, Xinmin Street, Changchun, 130021, Jilin Province, PR China

ARTICLE INFO

Keywords:
MicroRNA-200a
Fibroblast growth factor 7
Mitogen–activated protein kinase signaling pathway
Glaucoma
Retinal glial cell
Retinal ganglion cell

ABSTRACT

Glaucoma is a progressive optic neuropathy and is one of the leading causes of blindness in the industrialized countries. The involvement of microRNAs (miRs) has been implicated in regulating the complex biological responses to changes in intraocular pressure. However, the therapeutic role of miR-200a on glaucoma has not been well studied yet. In this study, we confirmed the role of miR-200a in glaucoma progression and identified the related mechanism. Microarray expression profiles were used to screen the glaucoma-related genes. The relationship between miR-200a and FGF7 was validated by bioinformatics analysis and dual-luciferase reporter gene assay. Glaucoma-related parameters including the expression of CD11b and iNOS, activation of Muller cells, and apoptosis of retinal ganglion cells (RGCs) in the mouse model were measured by immunohistochemistry, MTT assay and TUNEL assay, respectively. miR-200a was reduced in glaucoma, whereas FGF7 was robustly induced. Thereby, we speculated that FGF7 was negatively regulated by miR-200a. Downregulated miR-200a could activate the MAPK signaling pathway following elevations in ERK, JNK, p38 and Bax expression and reduction in Bcl-2 expression. In the mouse model, downregulated miR-200a increased the expression of CD11b and iNOS and the apoptosis of RGCs, but stimulated the inactivation of Muller cells. However, the above-mentioned alternations induced by downregulated miR-200a were reversed after FGF7 repression. miR-200a can inhibit the FGF7-mediated MAPK signaling pathway and play a protective role on improving the glaucoma-induced optical nerve injury.

1. Introduction

Glaucoma, a major cause of irreversible blindness worldwide, is characterized with progressive degeneration of the retinal ganglion cells (RGCs) consequently leading to impairment of the optic nerve and vision [1,2]. Glaucomatous optic neuropathy is estimated to affect > 60 million people worldwide with the incidence increasing to 76 million by 2020 and 111.8 million by 2040 [3]. Upregulated intraocular pressure (IOP) has been implicated among the many risk factors for glaucoma and involves in apoptosis-induced loss of RGCs [4]. Glial cells have been demonstrated to play a role in the pathogenesis of irreversible blindness [5]. Grieshaber et al. have verified overexpressed astrocytes and Muller cells in the retina of glaucoma [6]. Reactivation of Muller cells in glaucomatous retina may stimulate them to produce and release cytotoxic factors, ultimately leading to apoptosis and death of RGCs [7]. Hence, targeting the inactivation of Muller cells and survival of RGCs may be a more effective therapeutic strategy for treating glaucoma.

As a member of FGF family, fibroblast growth factor 7 (FGF7) is originally identified in mesenchymal cells. A previous study documented the involvement of FGF7 in the regeneration of epithelial tissues and stated that it is highly expressed in small-diameter dorsal root ganglion-origioned neurons [8]. Overexpression of FGF7 in the corneal epithelium is suggested to induce corneal intraepithelial neoplasia in young mice and epithelium hyperplasia in adult mice [9]. Another study shows that FGF7 is a mesenchyme-specific heparin-binding growth factor and can regulate numerous cellular and physiological processes by binding FGF receptor 2 (FGFR2) [10]. Zhang et al. shows

Abbreviations: miRs, MicroRNAs; RGCs, retinal ganglion cells; FGF7, fibroblast growth factor 7; GEO, Gene Expression Omnibus; NC, negative control; PBS, phosphate buffer saline; HE, Hematoxylin-eosin; DAB, diaminobenzidine; OD, optical density; RT-qPCR, Reverse transcription quantitative polymerase chain reaction; DEPC, diethyl pyrocarbonate; dNTP, deoxyribonucleoside triphosphate; DTT, dithiothreitol; RT, reverse transcription; SDS-PAGE, sodium dodecyl sulfate-polyacrylamide gel electrophoresis; TBS, tris-buffered saline; ECL, Enhanced chemiluminescence; FBS, fetal bovine serum; DMSO, dimethyl sulfoxide

* Corresponding author.
E-mail address: songedr@163.com (E. Song).

https://doi.org/10.1016/j.cellsig.2018.11.006
Received 24 July 2018; Received in revised form 7 November 2018; Accepted 9 November 2018
Available online 12 November 2018
0898-6568/

that the inhibition of the P2RX7/p38 MAPK pathway can inhibit oxidative stress-induced RGCs apoptosis in the treatment of glaucoma [11]. Furthermore, results of molecular modeling of HBA and Rac1-related signaling network highlighted the significance of the MAPK signaling pathway in reference to glaucoma [12].

MicroRNAs (miRNAs), a family of small noncoding RNA molecules, can regulate gene expression by binding to the complementary sites in the 3′-untranslated region of target messenger RNAs (mRNAs). They have been demonstrated to play pivotal roles in cell proliferation, differentiation, and apoptosis [13,14]. The dysregulation of miRNA expression has been identified in many eye disorders with one study estimating a correlation between the down-regulation of miR-182 expression by experimental autoimmune uveoretinitis and destruction of retinal structure [15]. In another study, miR-155, an immunologically relevant miRNA, was found to be poorly expressed in peripheral-blood mononuclear cells and dendritic cells of patients with Behcet's disease [16]. A previous study demonstrated the role of microRNA-200a (miR-200a) in regulating tumor progression in many types of tumors [17], while little is known about its function in glaucoma. Further, previous studies have highlighted the functionality of miRNAs in regulating p38 MAPK signaling pathway along the treatment of some diseases [18]. The inhibition of p38 MAPK signaling pathway in the retina may represent as a therapeutic target in the prevention of early pathogenesis in optic neuropathies [19]. Khaled et al. demonstrated that p38 MAPK inhibitor could stimulate the curative effect after glaucoma filtration surgery [20].

In the present study, we hypothesized that miR-200a may be a promising therapeutic target in glaucoma and the function of miR-200a on the activation of RGCs and apoptosis of RGCs was confirmed. Meanwhile, the role of FGF7 and MAPK signaling pathway was also detected.

2. Materials and methods

2.1. Ethics statement

All the experimental operations were performed with approval of the animal committee of the First Hospital of Jilin University. Significant efforts were made in order to minimize both the number of animals used as well as their respective suffering.

2.2. Acquisition and difference analysis of glaucoma expression chips

The glaucoma expression chip GSE2378 downloaded from the Gene Expression Omnibus (GEO) database (https://www.ncbi.nlm.nih.gov/geo/) included two platforms for sequencing data and the GPL8300 platform was utilized in the study. The Limma package of R language was applied to analyze the differences between the glaucoma samples and the normal controls with $|\log FC| > 2$ and p value $< .05$ as the threshold. A heatmap of the differentially expressed genes was obtained with pheatmap package of R language.

2.3. Retrieval of known genes and gene interaction analysis in glaucoma

The DisGeNET database (http://www.disgenet.org/web/DisGeNET/menu) was used to search for the known genes related to glaucoma. The STRING database (https://string-db.org/) was used to analyze the interaction between the known genes and the genes obtained from difference analysis. The Cytoscape software was used to establish the network diagram for gene interactions.

2.4. Prediction of regulatory miRNAs of FGF7

The regulatory miRNAs of FGF7 in the mice were predicted by the TargetScan database (http://www.targetscan.org/vert_71/), the miRNAMap database (http://mirnamap.mbc.nctu.edu.tw/) and the microRNA.org database (http://mirnamap.mbc.nctu.edu.tw/), respectively. The intersection of the results obtained from the above stated databases were analyzed in Venn diagram construction website (http://bioinformatics.psb.ugent.be/webtools/Venn/).

2.5. Dual-luciferase reporter gene assay

The biological prediction website microRNA.org was employed to analyze the target gene of miR-200a. The dual-luciferase reporter gene assay was performed to verify whether FGF7 is the direct target gene of miR-200a. In detail, 3'untranslated region (UTR) fragment of FGF7 was artificially synthesized and then introduced into the pGL3-control plasmid (Promega, Madison, WI, USA) *via* the endonuclease sites *Xho*I and BamH I. The mutant (Mut) site of complementary sequence of seed sequences on FGF7 wide type (Wt) plasmid was designed. After restriction endonuclease digestion, the target fragment was inserted into the pGL3-control plasmid using T4 DNA ligase. The Wt and Mut plasmids with correct sequences were separately co-transfected with miR-200a mimic or miR-200a negative control (NC) sequence into ARPE-19 cells (human retinal epithelial cells; Cell resources center, Shanghai Academy of life sciences, Chinese Academy of Sciences, Shanghai, China). The cells were collected and lysed after 48 h of transfection. The luciferase activity was measured using the Dual-Luciferase Reporter Assay System kit (Promega, Madison, WI, USA) on a TD-20/20 luminometer fluorescence detector (E5311, Promega, Madison, WI, USA).

2.6. Glaucoma model establishment

A total of 35 male C57BL/6 healthy mice (aged 8 to 10 weeks, weighing 25 g ± 2 g; Experimental Animal Center of Chongqing Medical University, Chongqing, China) were selected for this experiment. Especially, 30 mice served as the glaucoma group, whereas the remaining 5 mice were considered as the negative controls without any treatment. In detail, 0.5% Tobey was applied to the right eyes 30 min before the operation for mydriasis. Then, the mice were anesthetized with Avertin (0.5 mL/20 g) supplemented with 0.5% procaine eye drops. The surgery would be performed when the mouse was unresponsive to back pinching. Along the progression of the operation, the anterior chamber was punctured using a 31G needle from the lower limbus of the nose under a slit lamp microscope, which bypassed the iris and crystals. The aqueous humor was fully released during the operation, as to lower the anterior chamber and block the angle of the anterior chamber. Afterwards, a Hamilton syringe filled with 0.001 mL of air and 0.002 mL of Microbead sequentially infused the anterior chamber. After the operation, 0.5% erythromycin ointment was applied to the eyes. On the 5th day after establishment of the glaucoma model, the intraocular pressure of the mice was measured by a Goldmann applanation tonometer (Shanghai Precision Scientific Instruments Co., Ltd., Shanghai, China). After measuring, the model mice were transfected and grouped.

2.7. Mice grouping

The mice were assigned into 7 groups (5 mice/group): normal group (normal mice), blank control group (glaucoma mice without any treatment), NC group (glaucoma mice injected with miR-200a NC sequence), miR-200a mimic group (glaucoma mice injected with miR-200a mimic), miR-200a inhibitor group (glaucoma mice injected with miR-200a inhibitor), si-FGF7 group (glaucoma mice injected with FGF7 siRNA) and miR-200a inhibitor + si-FGF7 group (glaucoma mice injected with miR-200a inhibitor and FGF7 siRNA). Mice were fed coarse grain food and granted free access to water with 12 h light-dark cycle in natural light. Cholesterol-coated miR-200a mimic in phosphate buffer saline (PBS) (10 nM) was injected into the mice of the miR-200a mimic group *via* the cauda vein 5 min after remodeling, and miR-200a inhibitor lyophilized powder (10 nM) was injected into the mice in the

miR-200a inhibitor and miR-200a inhibitor + si-FGF7 groups *via* the cauda vein 3 days after modeling. Meanwhile, each mouse in the miR-200a inhibitor + si-FGF7 group was injected with 5 mg/(kg·L) FGF7 inhibitor. After the transfection, the mice in each group were sacrificed and tissues were extracted for subsequent experiments.

2.8. Retina tissue extraction

The right eyeball and the orbital optic nerves were completely extracted from the mice. The conjunctiva and muscle tissues were removed using a pair of micro-scissors and micro-tweezers, and immediately fixed with 10% neutral formaldehyde. After 24 h, the crystal was obtained through a limbus incision and fixed with 4% polyformaldehyde solution. After 48 h, paraffin sections (4 μm) were prepared with the above tissues using alcohol gradient, xylene and paraffin sequentially. The left eyeball was removed aseptically and washed three times with PBS to remove any peripheral fascia tissues. Then, the cornea, anterior segment tissues and vitreum were removed through an annular incision prepared 1 mm posterior to the corneoscleral edge. The retinal nerve epithelium layer was bluntly dissected from the eyecup using an ophthalmic micro-tweezer and completely incised into sections. The collected tissues were placed in a 15 mL centrifuge tube and centrifuged. A proportion of the supernatant was removed and the rest solution was stored for future use.

2.9. Hematoxylin-eosin (HE) staining

Paraffin sections were de-paraffinized two times with xylene (15 min per time), and then soaked two times in absolute ethyl alcohol (5 min per time), then 90% ethanol and 80% ethanol respectively (5 min per time). The sections were then stained with hematoxylin solution for 3 min after 3 PBS washes (5 min per time), followed by distilled water washing until the color of sections changed to blue. Then the sections were placed in 1% hydrochloric acid alcohol for 1 s for differentiation, followed by distilled water washing until the color of sections changed to blue. After washing, the sections were stained with eosin solution for 1 min. Then tissues were placed in gradient alcohol solution (70%, 80%, 90%, 100%, 100%) 2 min each time for dehydration, followed by xylene treatment two times (15 min per time), and sealed by neutral gum. The prepared sections were observed and photographed under the microscope (G600, Shenzhen Ze Sheng Yuan Technology Co., Ltd., Shenzhen, Guangdong, China). A morphological image analysis system (JD-801, Xiamen Baoneng Technology Co., Ltd., Xiamen, Fujian, China) was employed for analysis. The morphological changes in randomly selected fields were analyzed for each section at × 400 magnification.

2.10. Immunohistochemistry

The paraffin sections were de-paraffinized with xylene, washed under distilled water and treated with antigens according to the manufacturer's protocols (SPM120, Shanghai Mingrui Biotechnology Co., Ltd., Shanghai, China). In detail, the sections were firstly stained with PBS for 10 min, followed by 3% H_2O_2-methanol solution treatment for 10 min in order to remove the endogenous catalase. After washing the sections with PBS 3 times (2 min per time), the sections were covered with a drop of normal mouse serum for 10-minute incubation. After incubation, the serum were totally removed and each section was mounted with the rabbit anti-mouse antibodies to CD11b antibody (1:4000; ab133357, Abcam Inc., Cambridge, MA, USA) and inducible nitric oxide synthase (iNOS; 1:100; ab15323, Abcam Inc., Cambridge, MA, USA). The incubation was performed in a humid container for 30–60 min. After three times PBS washes (2 min per time), the sections were incubated with secondary antibody, biotin-labeled goat anti-mouse (ab205718, Abcam Inc., Cambridge, MA, USA) for 10 min. Subsequently, the sections were then mounted with streptavidin-peroxidase solution (Beijing Zhongshan Biotechnology Co., Ltd., Beijing, China) for 10 min after the PBS washes (2 min per time). Finally, the sections were added with a drop of the diaminobenzidine (DAB) chromogenic solution (Beijing Solarbio Science and Technology Co., Ltd., Beijing, China) for color development. The development was performed for 2–5 min at room temperature. Following being counter-stained with hematoxylin, the sections were differentiated with 0.1% hydrochloric acid and washed thoroughly under tap water to change the color to blue. Following dehydration by gradient alcohol, the sections were dried, treated with xylene and sealed with neutral gum. The sections were then observed under a microscope after being dried. The computer-image analyzer (CS-100A, Shenzhen Handenuo Electronics Technology Co., Ltd., Shenzhen, Guangdong, China) was employed to input the immunohistochemical section images through the acquisition system. A digital medical image analysis system (Motic Med 6.0, Shenzhen Shen Yuan Heng Science and Technology Co., Ltd., Shenzhen, Guangdong, China) was utilized for analyzing the optical density (OD) of the positive reaction sites in the images. The average OD value of positive cell staining was used to depict the antigen expression.

2.11. TdT-mediated dUTP-biotin nick end-labeling (TUNEL) staining

Five samples from the above dewaxed and washed sections were mounted with 50 μL of 1% proteinase K diluent, and incubated for 30 min at 37 °C, followed by three PBS washes (5 min per time). The sections were then mounted with 0.3% H_2O_2 methanol solution and incubated for 30 min at 37 °C. After 3 PBS washes (5 min per time), the sections were added with TUNEL reaction solution. The incubation was performed in a humid container for 1 h at 37 °C avoiding exposure to light. Then the sections were rinsed three times with PBS (5 min per time). A total of 50 μL of Converter-Peroxidase was trickled onto the sections, after which the samples were incubated in a wet box at 37 °C for 30 min. Following 3 PBS washes (5 min per time), the sections were incubated with the 2% DAB chromogenic solution at room temperature for 15 min. The reaction was terminated by addition of distilled water when cells showed brownish yellow nuclei under a microscope. Next, the sections were rinsed three times with PBS (5 min per time). Hematoxylin was employed for counter-staining and distilled water to subsequently terminate the reaction. Subsequently, the sections were dehydrated with gradient ethanol (50%, 70%, 90%, 100%), treated with xylene, followed by neutral gum mounting, and then observed under an optical microscope (× 400). The number of positive and negative cells was counted from 5 randomly selected fields in each section. Apoptotic cells were regarded as cells with tan nucleus, whereas those with blue nucleus were confirmed as normal cells. The apoptotic index (AI) was calculated as the ratio of the number of tan cells to that of the number of blue cells.

2.12. Reverse transcription quantitative polymerase chain reaction (RT-qPCR)

Total RNA from the mouse retina tissues was extracted according to the manufacturer's instructions of the Trizol kit (Invitrogen, Carlsbad, CA, USA). d The designed primers of miR-200a, FGF7, extracellular signal-regulated kinases (ERK), c-Jun N-terminal kinases (JNK) and p38 were synthesized by Oak Biotech Co., Ltd. (Zhenjiang, Jiangsu, China). The extracted RNA was dissolved in diethyl pyrocarbonate (DEPC) ultrapure water, and the OD value was measured with a Biochrom Ultrospec UV/Visible spectrophotometer (Biochrom, Cambourne, Cambridge, UK) at the wavelength of 260 nm and 280 nm. Meanwhile, the quality and concentration of total RNA was determined. The RNA template, primer mix, deoxyribonucleoside triphosphate (dNTP) mix, dithiothreitol (DTT), reverse transcription (RT) buffer, HiFi-MMLV and RNase-free water were dissolved on ice for later use. The reverse transcription system (20 μL) was prepared according to the manufacturer's instructions of the by TaqMan MicroRNA Assays Reverse

Table 1
Primer sequences for reverse transcription quantitative polymerase chain reaction.

Gene	Primer sequence
miR-200a	F: 5′-GAGTGCATCTTACCGGACAGT-3′
	R: 5′-GTGCAGGGTCCGAGGT-3′
FGF7	F: 5′-TGGGCACTATATCTCTAGCTTGC-3′
	R: 5′-GGGTGCGACAGAACAGTCT-3′
ERK	F: 5′-GCCTTACTCTACTTCTCCCCA-3′
	R: 5′-CTGCCTCTGACTTCTGAATGC-3′
JNK	F: 5′-CTCAGCATCCATCGTCTTCG-3′
	R: 5′-AGTCGGATCTGTGGACATTGA-3′
p38	F: 5′-GGACCTGAACAGGATCGTGAA-3′
	R: 5′-CTCAGCCATGAAGCCTCCC-3′
β-actin	F: 5′-GGCTGTATTCCCCTCCATCG-3′
	R: 5′-CCAGTTGGTAACAATGCCATGT-3′
U6	F: 5′-GCGCGTCGTGAAGCGTTC-3′
	R: 5′-GTGCAGGGTCCGAGGT-3′

Note: F, forward primer; R, reverse primer; FGF7, fibroblast growth factor 7; ERK, extracellular regulated protein kinase; JNK, C-Jun N-terminal kinase.

Transcription Primer (batch 4,366,596, Thermo Scientific, Waltham, MA, USA). The reaction conditions were set as follows: reverse transcription for 30–50 min at 42 °C and reverse transcriptase inactivation reaction for 5 s at 85 °C. The reaction solution was then subjected to fluorescence quantitative PCR using the SYBR® Premix Ex Taq™ II Kit (DRR041A, Beijing Zhijie Fangyuan Technology Co., Ltd., Beijing, China). The reaction system comprised of 25 μL of SYBR® Premix Ex Taq™ II (2 ×), 2 μL of PCR forward primer, 2 μL of PCR reserve primer, l μL of ROX Reference Dye (50 ×), 4 μL of DNA Template, and 16 μL of ddH_2O. Fluorescent quantitative PCR was then performed by an AM5000 Real-Time qPCR System (Shanghai Jitai Biotechnology Co., Ltd., Shanghai, China). The reactions conditions were as follows: predenaturation at 94 °C for 10 min, and then 40 cycles of denaturation at 94 °C for 15 s and annealing at 55 °C for 30 s, followed by final extension at 72 °C for 1 min. The primer sequences have been presented in Table 1. U6 was regarded as an internal reference for miR-200a, whereas β-actin was regarded for FGF7, ERK, JNK and p38. A solubility curve depicted the reliability of PCR results. The threshold cycle (CT) value was set and the relative expression of target gene was calculated by the $2^{-\Delta\Delta Ct}$ formula, in which

$$\Delta\Delta CT = \Delta Ct_{\text{experimental group}} - \Delta Ct_{\text{control group}}, \text{ and } \Delta Ct = Ct_{\text{target gene}} - Ct_{\text{internal reference}}.$$

2.13. Western blot analysis

Retinal tissues were immediately mixed with pre-cooled cell lysis buffer supplemented with 1% protease inhibitor, lysed on ice, and centrifuged at 12882 ×*g* for 30 min at 4 °C. The supernatant was collected for subsequent experimentation. Protein concentration was determined using the Bradford Kit (20201ES76, Shanghai Yeasen Biotech Co., Ltd., Shanghai, China). In each sample, 50 μg of protein was loaded and separated by sodium dodecyl sulfate-polyacrylamide gel electrophoresis (SDS-PAGE). After electrophoresis, the protein was transferred onto a nitrocellulose membrane (ZY-160FP, Shanghai Ze Ye Biological Technology Co., Ltd., Shanghai, China), followed by blocking with 5% skim milk powder for 2 h at room temperature. After three washes with tris-buffered saline (TBS) (10 min per time), the membrane was incubated with 1: 1000 diluted primary antibodies, rabbit anti-mouse polyclonal antibodies to FGF7 (sc-7882), JNK (ab179461), p-JNK (phospho T183 + T183 + T221; ab124956,), ERK (ab17942), p-ERK (phospho T185; ab214036), p38 (ab170099), p-p38 (ab47363), Bax (ab32503), and Bcl-2 (ab59348) and β-actin (ab8227) at 4 °C for one night. All the aforementioned antibodies were purchased from Abcam Inc. (Cambridge, MA, USA) except for FGF7 (Santa Cruz Biotechnology Inc., Santa Cruz, CA, USA). After incubation, the membrane was washed three times with TBS (10 min per time) at 37 °C, and incubated with the secondary antibody, goat anti-rabbit polyclonal antibody to IgG (1: 500; ab20272, Abcam Inc., Cambridge, MA, USA) labeled by horseradish peroxidase for 1 h at 37 °C. Enhanced chemiluminescence (ECL) solution (ECL808-25, Biomiga, Santiago, CA, USA) was added for development after three TBS washes. The procedure was performed at room temperature for 1 min. The membrane was then observed under an X-ray machine (OR-C302, Guangzhou Teeth Medical Devices Co., Ltd., Guangdong, China). The relative expression of the protein was calculated as the ratio of the gray value of the target band to that of the internal reference band.

2.14. Cultivation for Muller cells

One day before the cultivation, 2 mL of 100 μg/mL polylysine was uniformly applied to the cell culture flask. Then, the flask was stored in an incubator for 1 h at 37 °C, followed by removal of excessive polylysine, PBS rinsing and drying in the incubator for further use. The retinal nerve epithelial layer tissues were treated with 0.25% trypsin (ten times of the volume of the tissues) in a centrifuge tube immersed in a warm-water bath at 37 °C for 10 min. After trituration, the Muller cells were filtered through a 400-mesh filter. The filtrate was then centrifuged at 179 ×*g* for 5 min. The supernatant was removed. The collected precipitate was mixed with Dulbecco's modified eagle medium (DMEM)/F-12 medium supplemented with 10% fetal bovine serum (FBS). The cell suspension was prepared through trituration and incubation in the flask pre-coated with polylysine for one night at 37 °C with 5% CO_2. The medium was changed every 2 days. At 80% confluence, the cells were sub-cultured at a ratio of 1:2.

2.15. 3-(4,5-dimethylthiazol-2-yl)-2,5-diphenyltetrazolium bromide) (MTT) assay

Firstly, the density of Muller cells (the 3 - 4th generation) was adjusted to 1×10^6 cells/mL, and then inoculated to the 96-well culture plate at the density of 1×10^5 cells/well for two-day cultivation. The cells were treated with the aforementioned grouping. Five duplicated wells were set in each group including a blank well without any treatment. After cultivation for 24 h and 48 h, the cells were washed three times with DMEM/F-12 medium, mixed with 100 μL of MTT solution (5 mg/mL) in each well and incubated for 4 h at 37 °C with 5% CO_2. After discarding the MTT solution, the cells were mixed with 200 μL of dimethyl sulfoxide (DMSO), followed by vibration for 10 min. The mixture was allowed to react for 10 min, after which the OD value was measured using a microplate reader (Multiscan MK3, Thermo Fisher Scientific Inc., Waltham, MA, USA) at a wavelength of 570 nm at the 24th h, 48th h and 72nd h.

2.16. Statistical analysis

All data in this study were expressed as mean ± standard deviation. The statistical software (SPSS 18.0; IBM, New York, NY, USA) was used to analyze the data. One-way analysis of variance (ANOVA) was employed for comparisons among multiple groups, whereas *t*-test was employed for comparisons between two groups. A probability value $< .05$ was considered to be statistically significant.

3. Results

3.1. MiR-200a involves in the development of glaucoma by blocking the MAPK signaling pathway via FGF7

A total of 58 differentially expressed genes were obtained by comparing between glaucoma samples and normal controls in the glaucoma

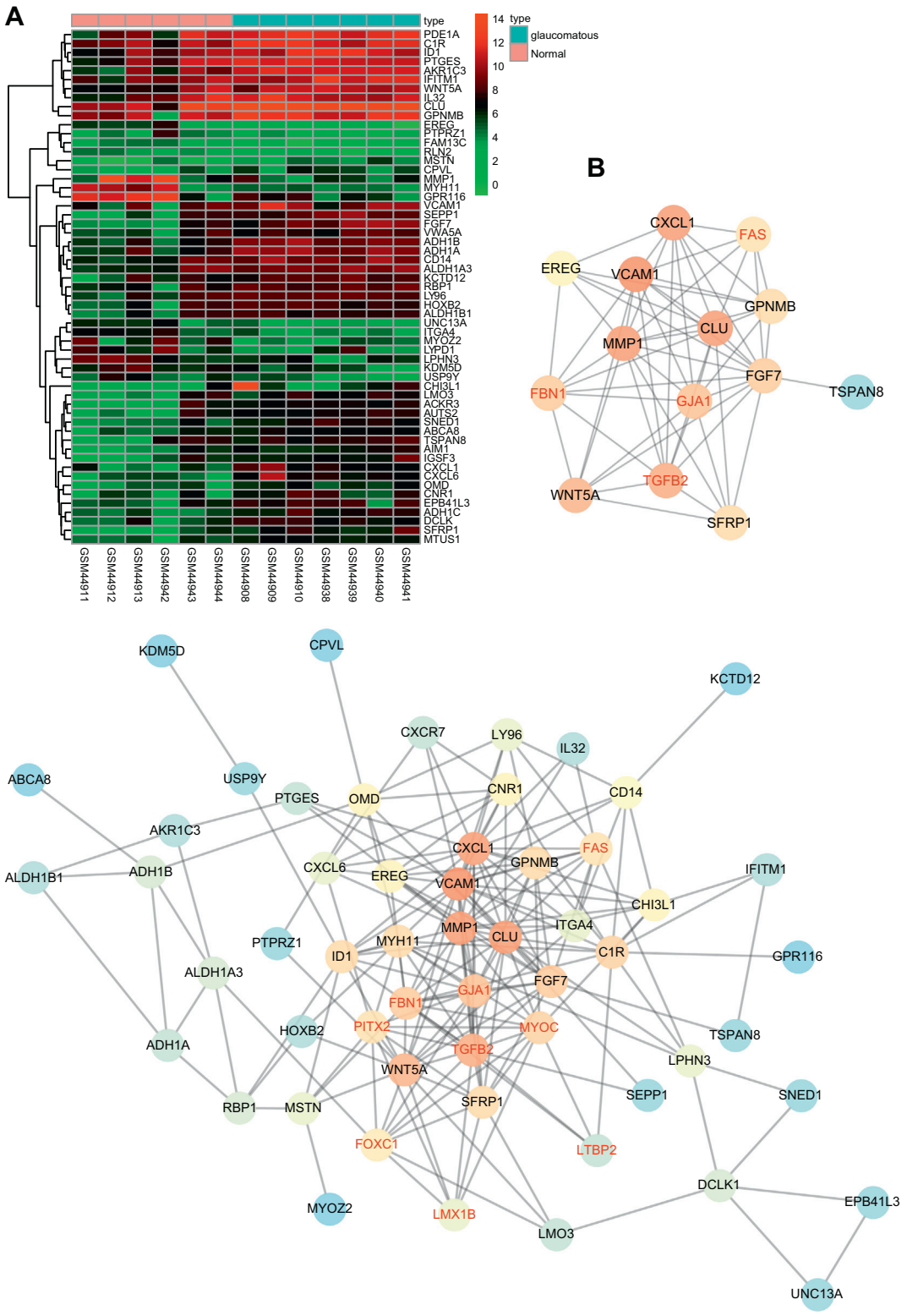

Fig. 1. FGF7 involves in the development of glaucoma. A, the differential analysis of glaucoma samples and normal controls in the chip. The abscissa indicates the sample number, the ordinate indicates the gene name, and the left dendrogram indicates the clustering of gene expression. Each box indicates the expression of a gene in one sample, and the upper right histograms represent the color orders; B, the analysis of diagram for gene interaction network. The first figure shows 58 different genes that are associated with 10 known genes, and the second figure represents genes that have direct or indirect effects on FGF7 genes in network maps. Each circle represents a gene. The color of the circle indicates the ranking of the gene in the network map. Especially, the gene with the closer links of FGF7 displays a brighter color. The font with red color indicates the known genes of glaucoma in the database, and the black indicates the differentially expressed genes obtained by differential analysis. (For interpretation of the references to color in this figure legend, the reader is referred to the web version of this article.)

Table 2
Glaucoma-related genes (Top 10).

Gene	Gene name	Score	PMIDs
LTBP2	Latent transforming growth factor beta binding pr...	0.402	8
SLC4A4	solute carrier family 4 member 4	0.4	2
MYOC	Myocilin	0.299	148
FOXC1	Forkhead box C1	0.214	24
PITX2	Paired like homeodomain 2	0.208	10
GJA1	Gap junction protein alpha 1	0.204	6
FBN1	Fibrillin 1	0.204	4
FAS	Fas cell surface death receptor	0.203	1
TGFB2	Transforming growth factor beta 2	0.202	9
LMX1B	LIM homeobox transcription factor 1 beta	0.202	6

Note: Score of the reliability of the gene-disease pair, based on the type and number of sources where is reported, and the number of PMIDs. PMIDs, total number of PMIDs supporting the association.

expression chip GSE2378. Especially, 44 genes were significantly upregulated compared to the normal controls, whereas another 14 genes were significantly downregulated ($p < .05$, Fig. 1A). Further, 10 genes with highest scores from the DisGeNET database were selected for subsequent analysis (Table 2). Meanwhile, the gene interaction network comprising of the aforementioned 58 genes and known genes was constructed in the STRING database (Fig. 1B). The results showed that matrix metalloproteinase 1 (MMP1) and FGF7 were the core genes among the 58 differentially expressed genes. The results of subsequent analysis demonstrated a correlation between FGF7 and the known glaucoma genes such as FBN1 and TGFB2, which was upregulated to its maximum potential within glaucoma samples. Therefore, FGF7 was chosen for our follow-up research. Previous studies revealed that FGF7 could act through the MAPK signaling pathway [21,22]. Moreover, existing researches has cited a correlation between the MAPK signaling pathway and the development of glaucoma [12,20,23]. Thus, we hypothesized that FGF7 may involve in the development of glaucoma through the MAPK signaling pathway. Further, regulatory miRNAs of FGF7 were predicted by databases and the results were shown in Fig. 2A. The intersection of the predicted results was also measured. In the microRNA.org database, only 40 regulatory miRNAs were predicted. Therefore, for intersection, only the top 40 miRNAs from the TargetScan and microRNA.org databases were selected. We found that 8 miRNAs were present in the intersection and the expressions of these 8 miRNAs in glaucoma mice were determined by RT-qPCR. The results of RT-qPCR showed that the expression of miR-200a in glaucoma samples varied sharply compared to the expressions of other miRNAs (Fig. 2B), supporting the regulatory role of miR-200a in glaucoma. The above findings suggested that miR-200a might mediate the MAPK signaling pathway and involve in the development of glaucoma *via* regulating FGF7.

3.2. FGF7 is a target gene of miR-200a

The target gene analysis of miR-200a was performed using the biological prediction site microRNA.org, which identified FGF7 as a direct target gene of miR-200a (Fig. 3A). The results showed that the transfection of miR-200a mimic significantly decreased the luciferase activity of the FGF7-Wt plasmid ($p < .05$) (Fig. 3B), which revealed that miR-200a inhibited the expression and functions of FGF7.

3.3. The structure and morphology of retina recovers by upregulated miR-200a or downregulated FGF7

In order to confirm the pathological changes of renal tissues, HE staining was performed. The normal group present with clear retinal layer (Fig. 4A) and thicker ganglion cell layer (GCL) (Fig. 4B). Compact and neatly arranged RGCs were observed with higher density (RGCD) (Fig. 4C) as well as normal structure and morphology. However, the structure and morphology of retinal cells in other groups changed distinctly with a decrease in nuclear density (all $p < .05$). In comparison with the blank controls, retinal cells in the miR-200a mimic group and the si-FGF7 group were relatively regular with increased RGCD ($p < .05$). In the miR-200a inhibitor group, the GCL was the thinnest with decreased RGCD and the least and loosest nuclei (all $p < .05$). No prominent changes in GCL, RGCD and number of nucleus were observed in the NC group and the miR-200a inhibitor + si-FGF7 group (all $p > .05$). The above results showed that the structure and morphology of retina recovered by upregulated miR-200a or downregulated FGF7.

3.4. Overexpression of miR-200a and silencing of FGF7 increased the expression of CD11b and iNOS

In order to identify the positive staining of microglia and average OD value of CD11b and iNOS in the optic nerve and retinal tissues, immunohistochemical assay was conducted (Fig. 5A–B). The results presented with no staining in CD11b and iNOS cells in the normal controls. However, a small amount of CD11b and iNOS cells were distributed in the miR-200a mimic and si-FGF7 groups. Meanwhile, the number of stained CD11b and iNOS cells increased in the blank controls, the NC group and the miR-200a inhibitor + si-FGF7 group. The miR-200a inhibitor group showed the largest number of stained CD11b and iNOS cells. The average OD value of CD11b and iNOS increased significantly in all other groups, except the normal controls ($p < .05$). In comparison with the blank controls, the average OD value of CD11b and iNOS decreased significantly in the miR-200a mimic and si-FGF7 groups ($p < .05$), whereas it increased obviously in the miR-200a

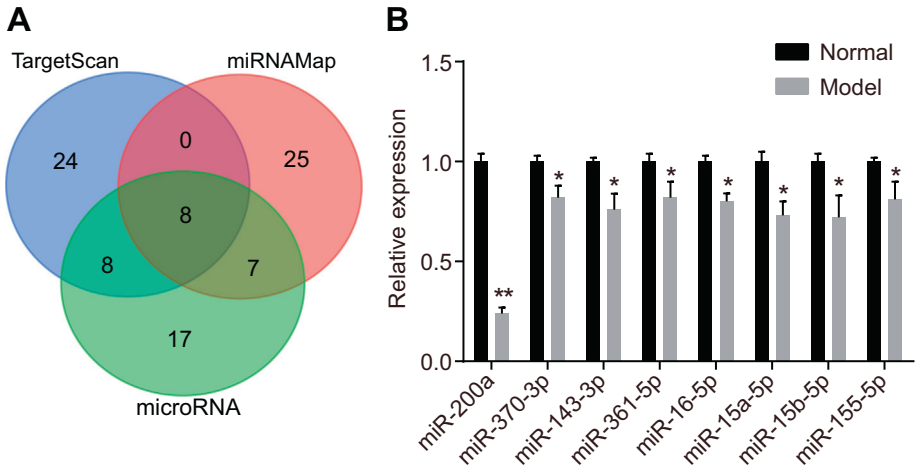

Fig. 2. MiR-200a is a regulatory miR of FGF7 in glaucoma. A, each circle in the graph represents a predicted result, and the overlapping part represents the intersection of predicted results. The numbers in the graph represent the number of miRNAs in each database; B, RT-qPCR was used to determine the expression of 8 miRNAs in mouse glaucoma samples and normal controls. *, $p < .05$ *vs.* the normal controls. *, $p < .01$ *vs.* the normal controls. MAPK, mitogen-activated protein kinase; FGF7, fibroblast growth factor 7; MMP1, matrix metalloproteinase; FBN1, fibrillin 1; TGFB2, transforming growth factor 2.

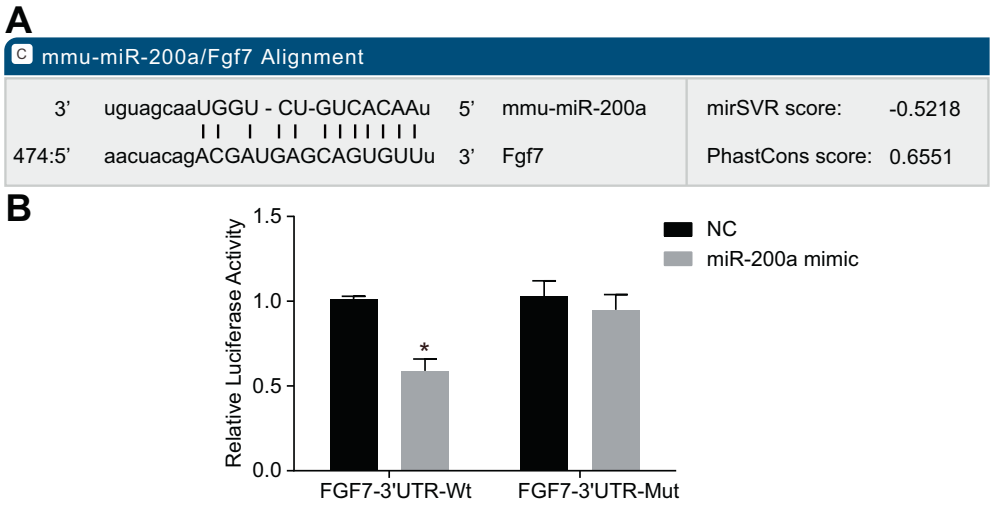

Fig. 3. MiR-200a targets FGF7. A, binding regions between FGF7 3'UTR and miR-200a sequence; B, luciferase activity of the FGF7 Wt and FGF7 Mut after transfection; NC, negative control; *, $p < .05$, *vs.* the NC group; data were expressed by means ± standard deviation and compared by *t*-test; the experiment was repeated 3 times.

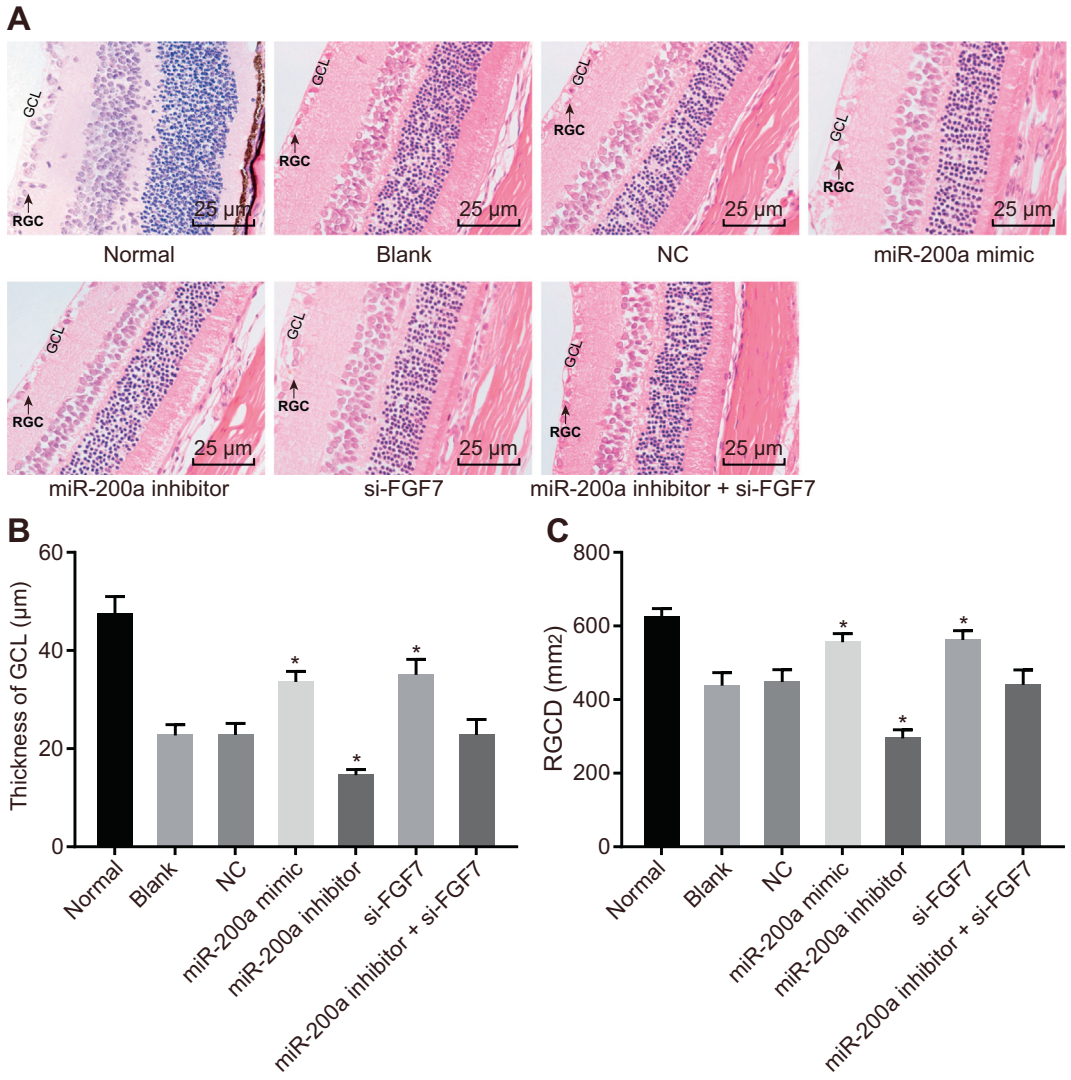

Fig. 4. The structure and morphology of retina recovers by upregulated miR-200a or downregulated FGF7. A, HE staining (400×) for frozen sections of retina, scale bar = 25 μm; B, thickness of GCL in cells treated with miR-200a mimic, miR-200a inhibitor and/or si-FGF7; C, RGCD of cells treated with miR-200a mimic, miR-200a inhibitor and/or si-FGF7; $n = 5$; *, $p < .05$ *vs.* the normal group; miR-200a, microRNA-200a; RGCs, retinal ganglion cells; NC, negative control; FGF7, fibroblast growth factor 7; si-FGF7, small interfering RNA against FGF7; HE, hematoxylin eosin; GCL, ganglion cell layer; RGCD, retinal ganglion cell density; data were expressed by means ± standard deviation; multiple groups were compared by one-way analysis of variance.

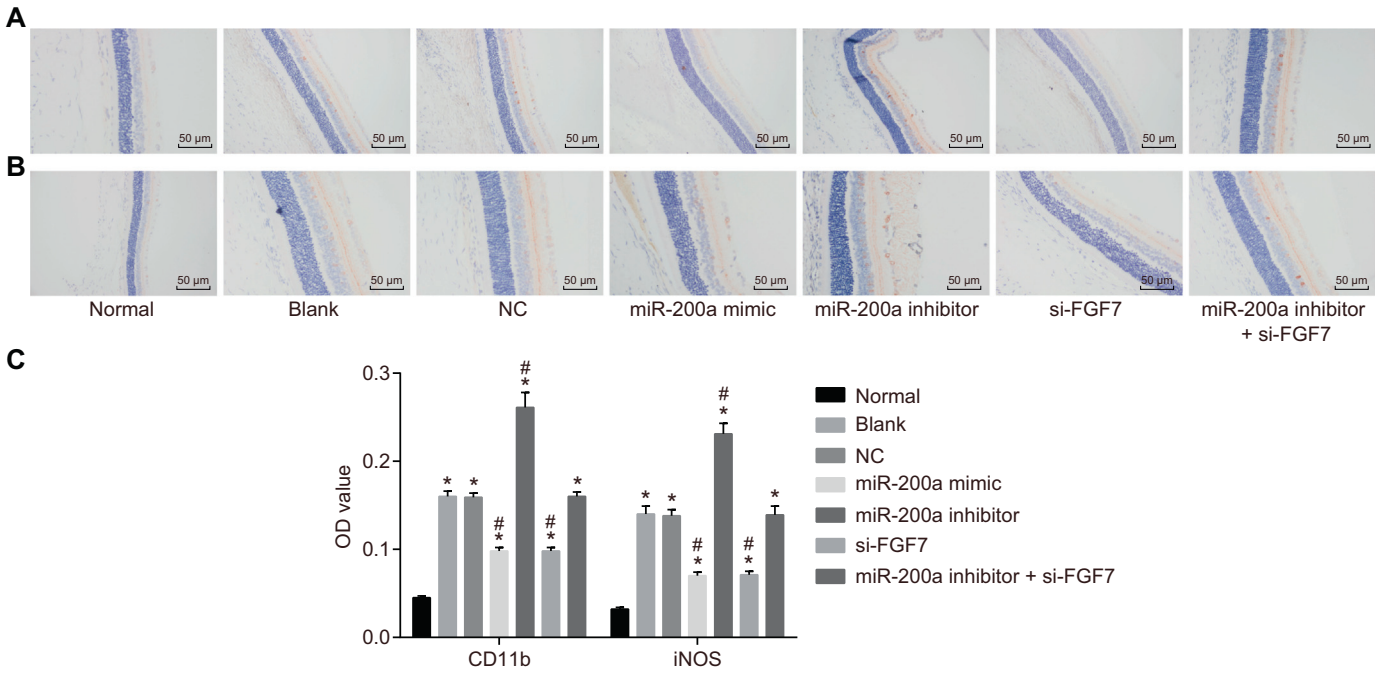

Fig. 5. Overexpression of miR-200a and silencing of FGF7 increases the expression of CD11b and iNOS. A, immunohistochemical staining of average OD value of CD11b in the optic nerve and retinal tissues (200 ×); B, immunohistochemical staining of average OD value of iNOS in the optic nerve and retinal tissues (200 ×); C, statistical analysis of the average OD value of CD11b and iNOS in different groups; miR-200a, microRNA-200a; RGCs, retinal ganglion cells; NC, negative control; FGF7, fibroblast growth factor 7; si-FGF7, small interfering RNA against FGF7; iNOS, inducible nitric oxide synthase; OD, optical value; *, $p < .05$ *vs.* the normal group; #, $p < .05$ *vs.* the blank group; $n = 5$; data were expressed by means ± standard deviation; multiple groups were compared by one-way analysis of variance.

inhibitor group ($p < .05$). No evident difference was observed in the average OD value of CD11b and iNOS between the NC and miR-200a inhibitor + si-FGF7 group ($p > .05$) (Fig. 5C). All these results implicated to the elevated expression of CD11b and iNOS due to overexpression of miR-200a or silencing of FGF7.

3.5. Overexpression of miR-200a and silencing of FGF7 inhibit the apoptosis of RGCs

Results of TUNEL assay showed that the apoptosis rates of RGCs in the mice retina were significantly increased compared to the rates observed in the normal controls ($p < .05$) (Fig. 6A - B). The apoptosis rates of RGCs in the miR-200a mimic group and the si-FGF7 group were remarkably decreased compared to that of the blank controls ($p < .05$), whereas the apoptosis rates increased greatly in the miR-200a inhibitor group ($p < .05$). However, no significant difference was observed in the apoptosis rates in the NC group and the miR-200a inhibitor + si-FGF7 group ($p > .05$). These findings provided evidence supporting that upregulated miR-200a or silenced FGF7 suppressed the apoptosis of RGCs.

3.6. MiR-200a suppressed the MAPK signaling pathway via downregulating FGF7

RT-qPCR results showed that miR-200a expression in retinal tissue decreased significantly compared to the expression in the normal controls ($p < .05$), whereas the mRNA levels of FGF7, ERK, JNK and p38 were increased ($p < .05$) (Fig. 7). The expression of miR-200a was significantly increased in the miR-200a mimic group in comparison with the blank controls ($p < .05$). However, no significant difference was observed in the normal controls and the si-FGF7 group ($p > .05$). The expression of miR-200a had significantly decreased in the miR-200a inhibitor group and the miR-200a inhibitor + si-FGF7 group ($p < .05$). The mRNA levels of FGF7, ERK, JNK and p38 decreased significantly in the miR-200a mimic group and the si-FGF7 group compared to those of the blank controls (all $p < .05$), whereas the levels were markedly increased in the miR-200a inhibitor group (all $p < .05$). Meanwhile, no significant difference was observed in the NC group and the miR-200a inhibitor + si-FGF7 group (all $p > .05$).

The results of Western blot analysis confirmed that protein levels of FGF7, ERK, JNK, p38 and Bax as well as the extents of JNK, ERK and p38 phosphorylation were significantly increased compared to those of the normal controls (all $p < .05$), whereas the protein levels of Bcl-2 had significantly decreased ($p < .05$) (Fig. 8A-B). Protein levels of FGF7, ERK, JNK, p38 and Bax as well as the extents of JNK, ERK and p38 phosphorylation were significantly decreased compared to those of the blank controls (all $p < .05$), whereas Bcl-2 had significantly increased in the miR-200a mimic group and the si-FGF7 group ($p < .05$). The miR-200a inhibitor group exhibited upregulated protein levels of FGF7, ERK, JNK, p38 and Bax along with up-regulated extents of JNK, ERK and p38 phosphorylation (all $p < .05$), and a downregulated protein level of Bcl-2 ($p < .05$). However, no significant difference was observed in the protein levels of FGF7, ERK, JNK, p38, Bax and Bcl-2 as well as the extent of JNK, ERK and p38 phosphorylation in the NC group and the miR-200a inhibitor + si-FGF7 group (all $p > .05$). The above results indicated that miR-200a could repress the MAPK signaling pathway *via* downregulating FGF7.

3.7. Overexpressed miR-200a could promote the viability of Muller cells by decreasing FGF7

Results of MTT assay (Fig. 9) revealed that there was no significant difference for OD_{570} of Muller cells in the retinal tissues at the 24th h ($p > .05$). However, when measuring at the 48th h and 72th h, OD_{570} was reduced significantly compared to that of the normal controls ($p < .05$). The OD_{570} of Muller cells in retinal tissues was significantly amplified in the miR-200a mimic group and the si-FGF7 group comparing to that of the blank controls ($p < .05$), whereas it decreased dramatically in the miR-200a inhibitor group ($p < .05$). Meanwhile, no significant difference was observed in the NC group and the miR-200a

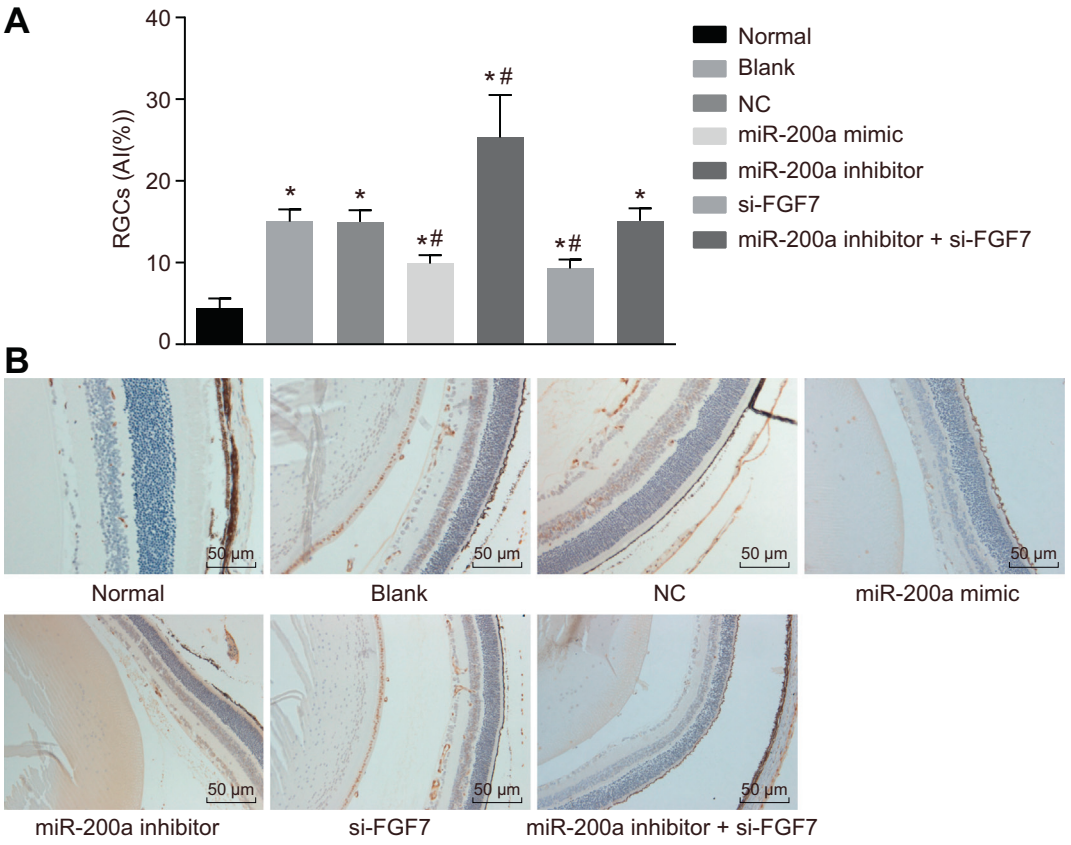

Fig. 6. Overexpression of miR-200a or silencing FGF7 leads to repressed RGC apoptosis. A, the apoptosis index of RGCs in each group; B, TUNEL staining reflecting apoptotic RGCs (as the arrow displaying); miR-200a, microRNA-200a; NC, negative control; FGF7, fibroblast growth factor 7; si-FGF7, small interfering RNA against FGF7; TUNEL, TdT-mediated dUTP-biotin nick end-labeling; RGCs, retinal ganglion cells; *, $p < .05$ *vs.* the normal group; #, $p < .05$ *vs.* the blank group; n = 5; data were expressed by means ± standard deviation; multiple groups were compared by one-way analysis of variance.

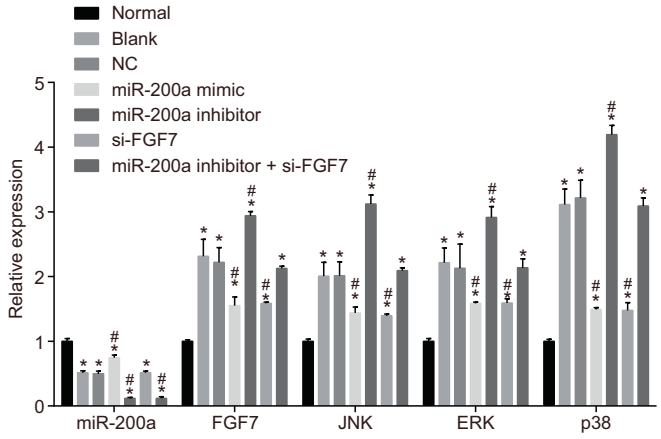

Fig. 7. miR-200a could downregulate the mRNA levels of FGF7, JNK, ERK and p38. miR-200a, microRNA-200a; NC, negative control; FGF7, fibroblast growth factor 7; si-FGF7, small interfering RNA against FGF7; MAPK, mitogen-activated protein kinase; RT-qPCR, reverse transcription quantitative polymerase chain reaction; *, $p < .05$ *vs.* the normal group; #, $p < .05$ *vs.* the blank group; data were expressed by means ± standard deviation; multiple groups were compared by one-way analysis of variance; the experiment was repeated 3 times.

inhibitor + si-FGF7 ($p > .05$). The above results revealed that overexpression of miR-200a could promote the viability of Muller cells *via* downregulating FGF7.

4. Supplementary result

The glaucoma models are successfully established: After the establishment of mouse glaucoma models, the IOP was changed. The IOP of the model group was significantly higher than that of the normal controls ($p < .05$) (Supplementary Fig. 1), supporting the reliability of the established glaucoma model.

5. Discussion

As the leading cause of irreversible blindness worldwide, glaucoma is featured by the progressive loss of axons in the optic nerve accompanied with damage to visual field [24]. Previous studies have demonstrated a relation between miRNAs with progressive optic neuropathy, which could serve as the prognostic tool in a clinical environment. Each miRNA possesses various potential targets; thus making it challenging to identify its *bona fide* targets. In this study, we aim to identify the regulatory role of miR-200a in glaucoma development. The results confirmed that miR-200a promoted the activation of retinal glial cells and inhibited the apoptosis of RGCs by suppressing the MAPK signaling pathway *via* downregulating FGF7.

Initially, our results demonstrated that the expression of miR-200a increased in mice with glaucoma, highlighting the significance of the role of played by miR-200a in glaucoma initiation and progression. The direct or indirect effects of miRNAs in glaucoma pathogenesis have been speculated. For example, miR-183 was identified to be upregulated in the retina of a mouse model with retinitis pigmentosa, which can alter the expression of intergrin-β1 and thereby have a cumulative effect on the physiology of trabecular meshwork (TM) leading to glaucoma [15,25]. One study showed that the expression of immune-

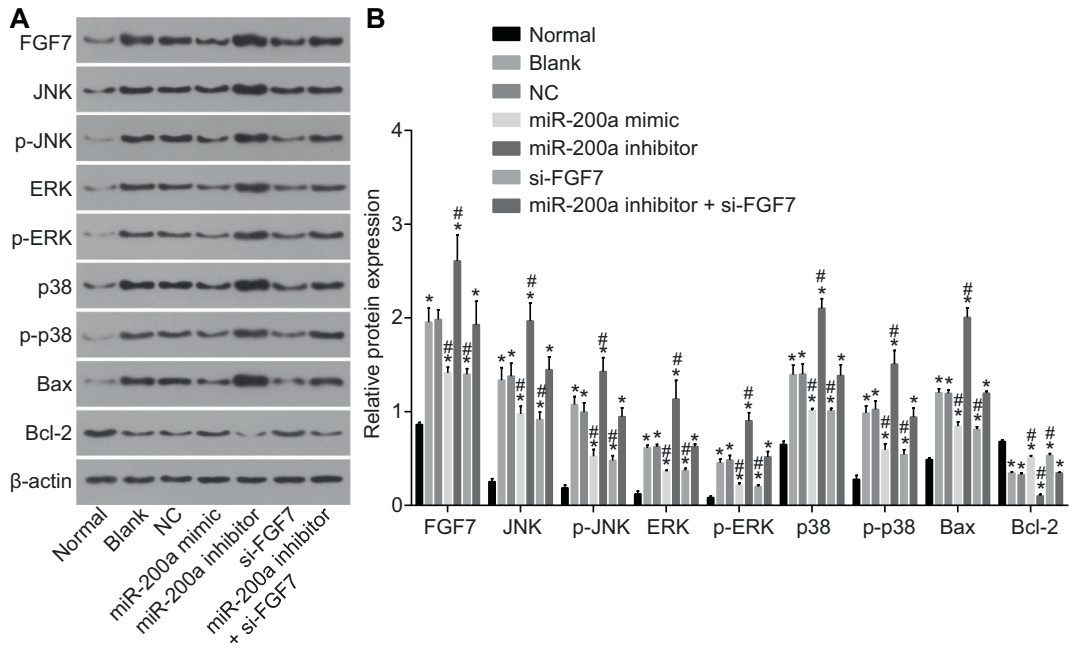

Fig. 8. miR-200a could reduce the protein levels of FGF7, JNK, ERK, p38, Bax and Bcl-2 as well as the extents of JNK, ERK and p38 phosphorylation. A, the gray values of FGF7, JNK, ERK, p38, Bax and Bcl-2, p-JNK, p-ERK, p-p38, Bax and Bcl-2 protein bands in response to the treatment of miR-200a mimic, miR-200a inhibitor and/or si-FGF7; B, the protein levels of FGF7, JNK, ERK, p38, Bax and Bcl-2 as well as the extents of JNK, ERK and p38 phosphorylation in response to the treatment of miR-200a mimic, miR-200a inhibitor and/or si-FGF7; miR-200a, microRNA-200a; NC, negative control; FGF7, fibroblast growth factor 7; si-FGF7, small interfering RNA against FGF7; MAPK, mitogen-activated protein kinase; RT-qPCR, reverse transcription quantitative polymerase chain reaction; *, $p < .05$ *vs.* the normal group; #, $p < .05$ *vs.* the blank group; data were expressed by means ± standard deviation; multiple groups were compared by one-way analysis of variance; the experiment was repeated 3 times.

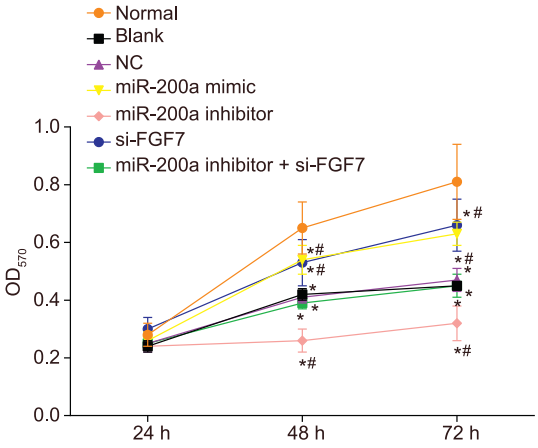

Fig. 9. Overexpressed miR-200a could elevate the viability of Muller cells by decreasing FGF7. MTT, 3-(4,5-dimethylthiazol-2-yl)-2,5-diphenyltetrazolium bromide; miR-200a, microRNA-200a; NC, negative control; FGF7, fibroblast growth factor 7; si-FGF7, small interfering RNA against FGF7; *, $p < .05$ *vs.* the normal group; #, $p < .05$ *vs.* the blank group; data were expressed by means ± standard deviation; multiple groups were compared by analysis of variance of repeated measurements; the experiment was repeated 3 times.

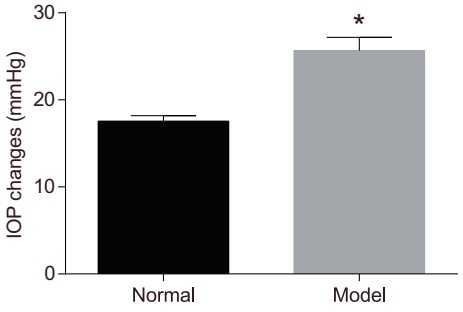

Supplementary Fig. 1. IOP changes verify the successful establishment of mouse models of glaucoma. IOP, intraocular pressure; *, $p < .05$ *vs.* the normal group; data were measurement data and analyzed by *t*-test; n = 5 in the normal group, $n = 30$ in the model group.

regulatory miRNAs such as miR-20a, -125b, -146a, -155, -181a, -223 and -17-92 complexes were higher in the plasma of patients with uveal melanoma [26]. Furthermore, another study found that miR-200a could downregulate the expression of aspartate-β-hydroxylase and inhibit the transition/cell proliferation of epithelial-mesenchymal in hepatoma cells *via* regulating ERK and PI3K/Akt pathways to [27]. On the basis of the target prediction program and the luciferase activity assay, our team of researchers demonstrated FGF7 as a putative target gene of miR-200a, which could be negatively targeted by miR-200a. The up-regulation of miR-200a could regulate the proliferation of adjacent cells by targeting gelsolin, which was a potent actin-severing protein and identified as the functional target of miR-200a [28].

In addition, our study revealed decreased expressions of FGF7, ERK, JNK, and p38, along with increased Bcl-2 due to the overexpression of miR-200a, indicating that miR-200a inactivates the MAPK signaling pathway *via* downregulating FGF7. A research by Jumpei et al. also confirmed that FGF7 could exercise its effects by regulating the MAPK signaling pathway [22]. Hani et al. reported that the upregulation of pro-apoptotic genes such as Bax and Bcl-2-associated death promoter could play a key role in the recovery of injured retinas and optic nerves [29]. RAF, MEK, and ERK proteins are major intracellular elements of the MAPK signaling pathway with various functions in cellular development, such as cell proliferation, differentiation and survival [30]. Curcumin has been demonstrated to exert antitumor effects in retinoblastoma cells by inducing the apoptosis of Y79 cells by activation of the JNK and p38 MAPK pathways [31]. In human uveal melanocytes, interleukin-1 increases the baseline expression and secretion of

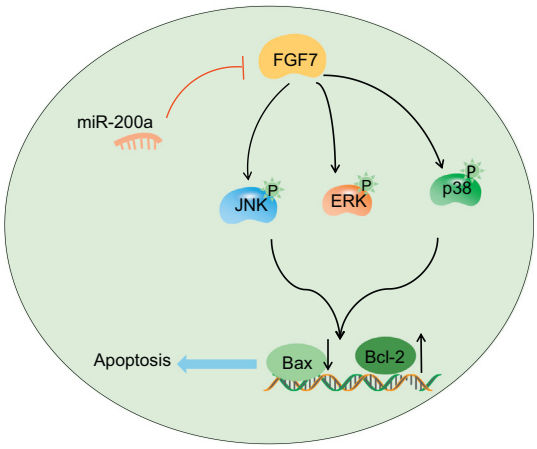

Fig. 10. MiR-200a mediated MAPK signaling pathway *via* targeting FGF7; FGF7 was downregulated by miR-200a *via* inhibiting the MAPK signaling pathway, resulting in downregulation of Bax expression and upregulation of Bcl-2 expression. Therefore, it inhibits the apoptosis of RGCs, relieves symptoms of glaucoma and ameliorates RGC apoptosis-induced glaucoma nerve injury.

interleukin-6 *via* the p38 MAPK/ NF-κB pathway *in vitro* [32].

Moreover, this study provided evidence that overexpression of miR-200a and silencing of FGF7 stimulates the activation of Muller cells and also inhibits the apoptosis of RGCs. In consistent with our results, a preexisting study showed that inactivated p38 MPAK pathway could contribute to the suppressed fibrotic tissue reaction in filtering glaucoma surgery [20]. Upregulated miR-200a has been reported to contribute in the suppression of cell growth [33]. The expression of miR-200a can be influenced by inactivation of p53 in pterygium, resulting in ZEB1/ZEB2 up-regulation and epithelial-mesenchymal transition (EMT) processing of pterygium [34]. It was also found that miR-200c can suppress the migration of retinoblastoma cells by stimulating the expression of E-cadherin. The miR-200c can also suppress the expression of Vimentin and N-cadherin in Y79 and Weri-rb1 cells [35].

6. Conclusions

Conclusively, our study demonstrated the involvement of miR-200a in glaucoma and RGCs apoptosis-induced optical nerve injury by downregulating FGF7, which suppresses the MAPK signaling pathway (Fig. 10). Therefore, the identification of miR-200a in the progression of glaucoma may aid in facilitating the existing understanding of the underlying mechanisms of glaucoma, with potential of serving as a prognostic marker for glaucoma treatments in the future. Meanwhile, the further investigation of the mechanism should be more scrupulously and logically performed with a diverse study population, so as to support a promising clinical application in treatment for glaucoma patients.

Author contributions

P.H. and S.Y.B. designed the study; H.J.L. and L.C.W. collated the data, designed and developed the database, carried out data analyses and produced the initial draft of the manuscript; and B.M.C. and S.E. contributed to drafting the manuscript. All authors read and approved the final manuscript.

Acknowledgments

The authors want to show their appreciation to the reviewers for their helpful comments.

Funding

None.

Conflict of interest declaration

None.

References

[1] Y. Jia, E. Wei, X. Wang, X. Zhang, J.C. Morrison, M. Parikh, L.H. Lombardi, D.M. Gattey, R.L. Armour, B. Edmunds, M.F. Kraus, J.G. Fujimoto, D. Huang, Optical coherence tomography angiography of optic disc perfusion in glaucoma, Ophthalmology 121 (7) (2014) 1322–1332.
[2] A. Bosco, M.R. Steele, M.L. Vetter, Early microglia activation in a mouse model of chronic glaucoma, J. Comp. Neurol. 519 (4) (2011) 599–620.
[3] B.M. Davis, L. Crawley, M. Pahlitzsch, F. Javaid, M.F. Cordeiro, Glaucoma: the retina and beyond, Acta Neuropathol. 132 (6) (2016) 807–826.
[4] P. Jha, H. Banda, R. Tytarenko, P.S. Bora, N.S. Bora, Complement mediated apoptosis leads to the loss of retinal ganglion cells in animal model of glaucoma, Mol. Immunol. 48 (15–16) (2011) 2151–2158.
[5] R.S. Chong, K.R. Martin, Glial cell interactions and glaucoma, Curr. Opin. Ophthalmol. 26 (2) (2015) 73–77.
[6] M.C. Grieshaber, F. Moramarco, A. Schoetzau, J. Flammer, S. Orguel, Detection of retinal glial cell activation in glaucoma by time domain optical coherence tomography, Klin. Monatsbl. Augenheilkd. 229 (4) (2012) 314–318.
[7] F. Gao, M. Ji, J.H. Wu, Z.F. Wang, [Roles of retinal Muller cells in health and glaucoma], Sheng Li Xue Bao 65 (6) (2013) 654–663.
[8] H. Liu, Q.F. Wu, J.Y. Li, X.J. Liu, K.C. Li, Y.Q. Zhong, D. Wu, Q. Wang, Y.J. Lu, L. Bao, X. Zhang, Fibroblast growth factor 7 is a nociceptive modulator secreted via large dense-core vesicles, J. Mol. Cell Biol. 7 (5) (2015) 466–475.
[9] T. Chikama, C.Y. Liu, J.T. Meij, Y. Hayashi, I.J. Wang, L. Yang, T. Nishida, W.W. Kao, Excess FGF-7 in corneal epithelium causes corneal intraepithelial neoplasia in young mice and epithelium hyperplasia in adult mice, Am. J. Pathol. 172 (3) (2008) 638–649.
[10] T. Huang, L. Wang, D. Liu, P. Li, H. Xiong, L. Zhuang, L. Sun, X. Yuan, H. Qiu, FGF7/FGFR2 signal promotes invasion and migration in human gastric cancer through upregulation of thrombospondin-1, Int. J. Oncol. 50 (5) (2017) 1501–1512.
[11] Q.L. Zhang, W. Wang, Y. Jiang, A. Tuya, L.L. Dongmei, Z.J. Lu Li, H. Chang, T.Z. Zhang, GRGM-13 comprising 13 plant and animal products, inhibited oxidative stress induced apoptosis in retinal ganglion cells by inhibiting P2RX7/p38 MAPK signaling pathway, Biomed. Pharmacother. 101 (2018) 494–500.
[12] L. Cao, L. Wang, G. Cull, A. Zhou, Alterations in molecular pathways in the retina of early experimental glaucoma eyes, Int. J. Physiol. Pathophysiol. Pharmacol 7 (1) (2015) 44–53.
[13] J. Cai, X. Liu, J. Cheng, Y. Li, X. Huang, Y. Li, X. Ma, H. Yu, H. Liu, R. Wei, MicroRNA-200 is commonly repressed in conjunctival MALT lymphoma, and targets cyclin E2, Graefes Arch. Clin. Exp. Ophthalmol. 250 (4) (2012) 523–531.
[14] Z. Zhang, X. Luo, S. Ding, J. Chen, T. Chen, X. Chen, H. Zha, L. Yao, X. He, H. Peng, MicroRNA-451 regulates p38 MAPK signaling by targeting of Ywhaz and suppresses the mesangial hypertrophy in early diabetic nephropathy, FEBS Lett. 586 (1) (2012) 20–26.
[15] A. Raghunath, E. Perumal, Micro-RNAs and their roles in eye disorders, Ophthalmic Res. 53 (4) (2015) 169–186.
[16] Q. Zhou, X. Xiao, C. Wang, X. Zhang, F. Li, Y. Zhou, A. Kijlstra, P. Yang, Decreased microRNA-155 expression in ocular Behcet's disease but not in Vogt Koyanagi Harada syndrome, Invest. Ophthalmol. Vis. Sci. 53 (9) (2012) 5665–5674.
[17] Y. Chen, W. Peng, Y. Lu, J. Chen, Y.Y. Zhu, T. Xi, MiR-200a enhances the migrations of A549 and SK-MES-1 cells by regulating the expression of TSPAN1, J. Biosci. 38 (3) (2013) 523–532.
[18] K. Murata, H. Yoshitomi, M. Furu, M. Ishikawa, H. Shibuya, H. Ito, S. Matsuda, MicroRNA-451 down-regulates neutrophil chemotaxis via p38 MAPK, Arthritis Rheum. 66 (3) (2014) 549–559.
[19] J.D. Dapper, S.D. Crish, I.H. Pang, D.J. Calkins, Proximal inhibition of p38 MAPK stress signaling prevents distal axonopathy, Neurobiol. Dis. 59 (2013) 26–37.
[20] K. Nassar, A. Tura, J. Luke, M. Luke, S. Grisanti, S. Grisanti, A p38 MAPK inhibitor improves outcome after glaucoma filtration surgery, J. Glaucoma 24 (2) (2015) 165–178.
[21] J.E. Fata, H. Mori, A.J. Ewald, H. Zhang, E. Yao, Z. Werb, M.J. Bissell, The MAPK (ERK-1,2) pathway integrates distinct and antagonistic signals from TGFalpha and FGF7 in morphogenesis of mouse mammary epithelium, Dev. Biol. 306 (1) (2007) 193–207.
[22] J. Terakawa, A. Rocchi, V.A. Serna, E.P. Bottinger, J.M. Graff, T. Kurita, FGFR2IIIb-MAPK activity is required for epithelial cell fate decision in the lower Mullerian Duct, Mol. Endocrinol. 30 (7) (2016) 783–795.
[23] J.N. Bailey, B.L. Yaspan, L.R. Pasquale, M.A. Hauser, J.H. Kang, S.J. Loomis, M. Brilliant, D.L. Budenz, W.G. Christen, J. Fingert, D. Gaasterland, T. Gaasterland, P. Kraft, R.K. Lee, P.R. Lichter, Y. Liu, C.A. McCarty, S.E. Moroi, J.E. Richards, T. Realini, J.S. Schuman, W.K. Scott, K. Singh, A.J. Sit, D. Vollrath, G. Wollstein, D.J. Zack, K. Zhang, M.A. Pericak-Vance, R.R. Allingham, R.N. Weinreb, J.L. Haines, J.L. Wiggs, Hypothesis-independent pathway analysis implicates GABA and acetyl-CoA metabolism in primary open-angle glaucoma and normal-pressure glaucoma, Hum. Genet. 133 (10) (2014) 1319–1330.

[24] E.N. Vithana, C.C. Khor, C. Qiao, M.E. Nongpiur, R. George, L.J. Chen, T. Do, K. Abu-Amero, C.K. Huang, S. Low, L.A. Tajudin, S.A. Perera, C.Y. Cheng, L. Xu, H. Jia, C.L. Ho, K.S. Sim, R.Y. Wu, C.C.Y. Tham, P.T.K. Chew, D.H. Su, F.T. Oen, S. Sarangapani, N. Soumittra, E.A. Osman, H.T. Wong, G. Tang, S. Fan, H. Meng, D.T.L. Huong, H. Wang, B. Feng, M. Baskaran, B. Shantha, V.L. Ramprasad, G. Kumaramanickavel, S.K. Iyengar, A.C. How, K.Y. Lee, T.A. Sivakumaran, V.H.K. Yong, S.M.L. Ting, Y. Li, Y.X. Wang, W.T. Tay, X. Sim, R. Lavanya, B.K. Cornes, Y.F. Zheng, T.T. Wong, S.C. Loon, V.K.Y. Yong, N. Waseem, A. Yaakub, K.S. Chia, R.R. Allingham, M.A. Hauser, D.S.C. Lam, M.L. Hibberd, S.S. Bhattacharya, M. Zhang, Y.Y. Teo, D.T. Tan, J.B. Jonas, E.S. Tai, S.M. Saw, D.N. Hon, S.A. Al-Obeidan, J. Liu, T.N.B. Chau, C.P. Simmons, J.X. Bei, Y.X. Zeng, P.J. Foster, L. Vijaya, T.Y. Wong, C.P. Pang, N. Wang, T. Aung, Genome-wide association analyses identify three new susceptibility loci for primary angle closure glaucoma, Nat. Genet. 44 (10) (2012) 1142–1146.
[25] G. Li, C. Luna, J. Qiu, D.L. Epstein, P. Gonzalez, Targeting of integrin beta1 and kinesin 2alpha by microRNA 183, J. Biol. Chem. 285 (8) (2010) 5461–5471.
[26] S. Achberger, W. Aldrich, R. Tubbs, J.W. Crabb, A.D. Singh, P.L. Triozzi, Circulating immune cell and microRNA in patients with uveal melanoma developing metastatic disease, Mol. Immunol. 58 (2) (2014) 182–186.
[27] W.F. Yao, J.W. Liu, D.S. Huang, MiR-200a inhibits cell proliferation and EMT by down-regulating the ASPH expression levels and affecting ERK and PI3K/Akt pathways in human hepatoma cells, Am. J. Transl. Res. 10 (4) (2018) 1117–1130.
[28] Y. Xu, Y. Zhang, L. Wang, R. Zhao, Y. Qiao, D. Han, Q. Sun, N. Dong, Y. Liu, D. Wu, X. Zhang, N. Huang, N. Ma, W. Zhao, Y. Liu, X. Gao, miR-200a targets gelsolin: a novel mechanism regulating secretion of microvesicles in hepatocellular carcinoma cells, Oncol. Rep. 37 (5) (2017) 2711–2719.
[29] H. Levkovitch-Verbin, D. Makarovsky, S. Vander, Comparison between axonal and retinal ganglion cell gene expression in various optic nerve injuries including glaucoma, Mol. Vis. 19 (2013) 2526–2541.
[30] B. Di Benedetto, C. Hitz, S.M. Holter, R. Kuhn, D.M. Vogt Weisenhorn, W. Wurst, Differential mRNA distribution of components of the ERK/MAPK signalling cascade in the adult mouse brain, J. Comp. Neurol. 500 (3) (2007) 542–556.
[31] X. Yu, J. Zhong, L. Yan, J. Li, H. Wang, Y. Wen, Y. Zhao, Curcumin exerts antitumor effects in retinoblastoma cells by regulating the JNK and p38 MAPK pathways, Int. J. Mol. Med. 38 (3) (2016) 861–868.
[32] D.N. Hu, M. Chen, D.Y. Zhang, F. Ye, S.A. McCormick, C.C. Chan, Interleukin-1beta increases baseline expression and secretion of interleukin-6 by human uveal melanocytes in vitro via the p38 MAPK/NF-kappaB pathway, Invest. Ophthalmol. Vis. Sci. 52 (6) (2011) 3767–3774.
[33] S.L. Gao, L.Z. Wang, H.Y. Liu, D.L. Liu, L.M. Xie, Z.W. Zhang, miR-200a inhibits tumor proliferation by targeting AP-2gamma in neuroblastoma cells, Asian Pac. J. Cancer Prev. 15 (11) (2014) 4671–4676.
[34] C.W. Wu, M.L. Peng, K.T. Yeh, Y.Y. Tsai, C.C. Chiang, Y.W. Cheng, Inactivation of p53 in pterygium influence miR-200a expression resulting in ZEB1/ZEB2 up-regulation and EMT processing, Exp. Eye Res. 146 (2016) 206–211.
[35] X.L. Shao, Y. Chen, L. Gao, MiR-200c suppresses the migration of retinoblastoma cells by reversing epithelial mesenchymal transition, Int. J. Ophthalmol. 10 (8) (2017) 1195–1202.